State Dynamics and Modeling of Tantalum Oxide Memristors

John Paul Strachan, *Member, IEEE*, Antonio C. Torrezan, *Member, IEEE*, Feng Miao, Matthew D. Pickett, J. Joshua Yang, *Member, IEEE*, Wei Yi, Gilberto Medeiros-Ribeiro, and R. Stanley Williams, *Senior Member, IEEE*

***Abstract*— A key requirement for using memristors in circuits is a predictive model for device behavior that can be used in simulations and to guide designs. We analyze one of the most promising materials, tantalum oxide, for high density, low power, and high-speed memory. We perform an ensemble of measurements, including time dynamics across nine decades, to deduce the underlying state equations describing the switching in Pt/TaO_x/Ta memristors. A predictive, compact model is found in good agreement with the measured data. The resulting model, compatible with SPICE, is then used to understand trends in terms of switching times and energy consumption, which in turn are important for choosing device operating points and handling interactions with other circuit elements.**

***Index Terms*— Crossbar, device dynamics, memristor, resistive memory (RRAM), SPICE.**

I. Introduction

OXIDE-BASED resistance switching devices have the potential to fulfill the performance requirements for a universal memory: nonvolatility, high-speed, high-density, and low-energy operation. These devices are dynamical passive elements that display the electronic circuit properties of a memristor [1]–[4]. In addition to nonvolatile memory, such devices are proposed for a variety of other applications, including logic, hybrid circuits with CMOS, and neuromorphic computing. Among the resistance switching materials so far studied, tantalum oxide shows favorable resistance switching properties, particularly endurance, voltage and current levels, speed of switching, energy cost to switch, and materials compatibility with back end of the line processing with CMOS. Several research groups, including the present authors, studied this system and reported write/erase endurance demonstrations, high speed with low-energy switching, multilevel analog states, using a threshold switching layer to reduce sneak paths in crossbars, and long retention time [5]–[12].

A prototype memory circuit using the tantalum oxide material system and a threshold switch was demonstrated [13]. However, to optimize the performance of such a system, a predictive and accurate device model is required for circuit design and simulation in large crossbar arrays. The first example based on the memristor formalism was a highly simplified vacancy drift model used to demonstrate the concept of a state variable in a dynamical electronic circuit element based on TiO_2 [14]. Many researchers adapted this model in a variety of ways, including applying it to TaO_x devices [15]. Subsequently, other compact resistance switching device models were developed and applied in several cases [16]–[23]. The actual ionic motion in an oxide can involve a complicated interplay of drift, diffusion, and thermophoresis [24], [25], and for the case of TiO_2 a detailed experimental analysis revealed an extremely nonlinear current–voltage and dynamical switching behavior. A simple model was proposed that satisfied both the electronic measurements and the materials composition of the device [18], but we have observed that the TaO_x system is very different from TiO_2, both in electrical and structural characteristics.

The goal of this paper is to provide a compact model for TaO_x memristors that is strongly grounded in experimental data. Our model is developed by performing a detailed study of the electronic transport and switching dynamics data spanning nine decades in time for both OFF and ON switching. The resulting device model constrains some of the underlying physical mechanisms for explaining the switching in tantalum oxide [15], [22], [26], and we explore the ramifications of the device behavior for switching speed, energy, and the interplay with varying circuit environments.

II. Experiment

A. Materials

The materials stack for devices in this paper consists of a thin (4–10 nm) amorphous, nearly stoichiometric Ta_2O_{5-x} film between an inert Pt electrode and a Ta electrode, identical to that used in [9] and [10]. As shown in Fig. 1, such a structure shows bipolar resistive switching with a nearly linear low-resistance (ON) state and increasing nonlinearity in higher resistance (OFF) states. Although high-voltage electroforming [5]–[7] is eliminated in this structure, the first ON-switching voltage is higher than average (Fig. 1) and permanently reduces the device resistance from the as-fabricated high-impedance state.

Manuscript received December 7, 2012; revised April 11, 2013; accepted May 15, 2013. Date of current version June 17, 2013. This work was supported in part by the U.S. Government's Nano-Enabled Technology Initiative. The review of this paper was arranged by Editor G. Jeong.

The authors are with the Hewlett-Packard Labs, Palo Alto, CA 94304 USA (e-mail: john-paul.strachan@hp.com).

Color versions of one or more of the figures in this paper are available online at http://ieeexplore.ieee.org.

Digital Object Identifier 10.1109/TED.2013.2264476

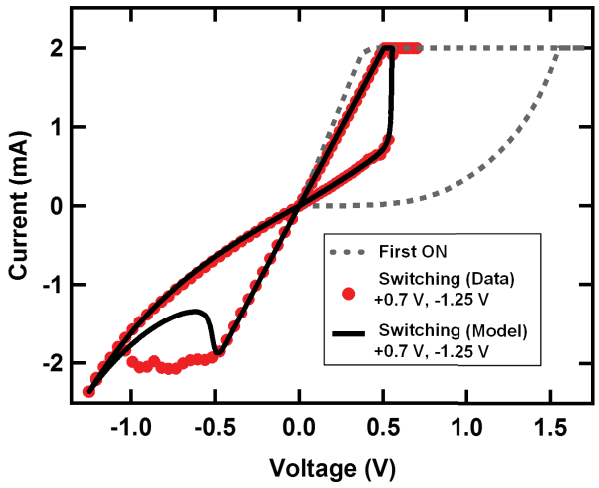

Fig. 1. Representative current–voltage curve for a TaO_x memristor showing bipolar switching following an initial +1.8-V sweep ON. Solid line: simulation results using the measured initial conditions and applying an identical voltage cycle to the device, including a +2-mA current compliance.

B. Memristor Modeling

Letting y denote the state variable for a tantalum oxide memristor, the key equations describing the quasi-static conduction (state-dependent Ohm's Law) and the dynamics of the state variable are given by the Chua memristor equations [2] as follows:

$$i(t) = G(y, v)v(t) \tag{1}$$

$$\frac{dy(t)}{dt} = F(y, v) \tag{2}$$

where $G(y, v)$ is the (possibly voltage dependent) conductance for a given memristor state y, and $F(y, v)$ describes the dynamical evolution of the state. To determine an analytical approximation to $G(y, v)$, we perform static measurements of the current–voltage dependence in a variety of memristor states y using voltages too small to cause detectable switching. For extracting the $F(y, v)$ dynamics, we carried out time-dependent measurements with varying voltage v and initial conditions.

C. Physical Picture

To understand the nature of the transport in tantalum oxide memristors, physical characterization of devices following operation has been carried out. Although the complete picture is still evolving, several issues are apparent: 1) transport, at least in the ON state, is dominated by a channel, or subregion, of the device; 2) the region within and surrounding the active channel shows modification of the original Ta:O ratio with oxygen partially depleted within the channel [26], [27] and having a slightly higher concentration outside; and 3) modification of the structure surrounding the channel, in particular a nanocrystalline phase evolving from the initially deposited amorphous film, indicating local heating. Viewed in a direction perpendicular to the sample plane, the pattern of the oxygen depletion has a particular configuration, as shown schematically in Fig. 2(a), in which the effective thickness of

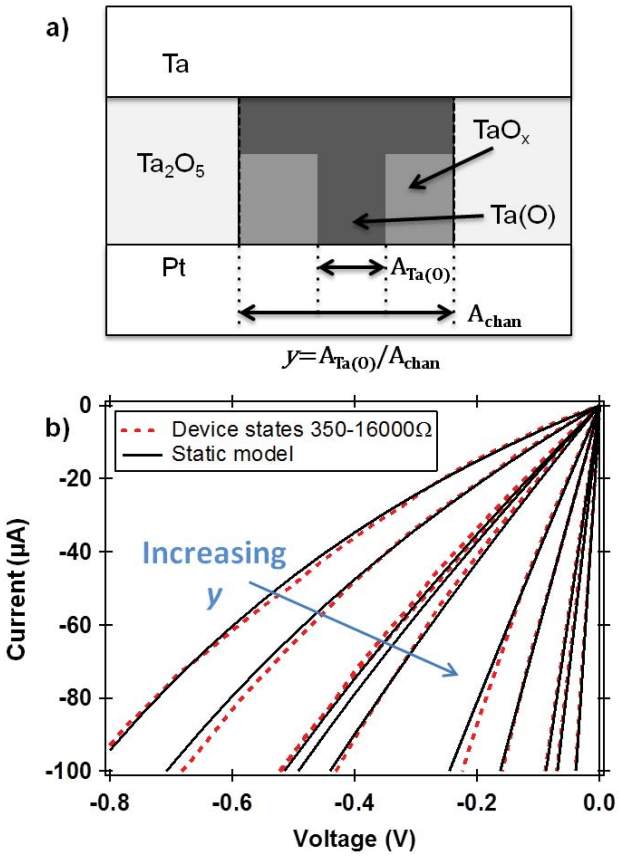

Fig. 2. (a) Schematic view representation of tantalum oxide memristor based on prior physical characterization (see text). (b) Electrical measurements of device states spanning 35 Ω–16 kΩ with bias low enough to avoid switching. Solid lines show the fitted static model results.

the film is reduced, with the remaining gap depleted in oxygen relative to the as-grown composition [26]. This geometry for the active channel allows several conductance regimes. In the extreme cases, the full thickness is either stoichiometric Ta_2O_5 or Ta with dissolved O (referred to as Ta(O), with solubility up to 20%), the two thermodynamically stable phases in the Ta-O system, to give an insulating or metallic channel, respectively. By either combining these two phases in parallel, or considering Ta(O) with different concentrations of O, there is a range of stable intermediate conductance states [28] available to the device.

D. Static (Nonswitching) Data and Model

The results reported here, along with a complementary study of transport as a function of composition in tantalum oxide films [29], indicate that the key parameter to describe the memristor state is the oxygen content in a conducting channel, and this has guided the choice of state variable in this paper. It is not conclusively known whether the device states strictly reflect a varying Ta:O ratio in a compositionally uniform channel, or a varying ratio of two different oxygen compositions Ta(O) versus Ta_2O_5. Electrically, they are indistinguishable, hence for convenience we use a model with the two phases in parallel. The state variable y is thus the volume fraction (or equivalently cross-sectional area) of the

channel with metallic transport, i.e., linear current–voltage dependence and positive thermal coefficient of resistance. The remaining fractional volume $1-y$ is insulating with a nonlinear transport (described below) and a negative thermal coefficient of resistance. Temperature-dependent transport studies were performed on extremal device states, verifying that the ON state was metallic, whereas the OFF state transport was best described by a nonlinear Frenkel–Poole relationship. Thus, the device conductance is approximated by the parallel combination of the two phases, shown in Fig. 2(a) and given by the equation,

$$i = v[yG_m + (1-y)a\exp[b\sqrt{|v|}] \tag{3}$$

where G_m, a, and b are constants for a particular device across all states and cycling history, and depend on the material properties within the conduction channel. The conductance of the device is G_m when the linear metallic Ta(O) phase fills the entire channel, and thus $y = 1$. The second term describes the Frenkel–Poole transport when the more oxidized phase fills the entire channel, and thus $y = 0$.

A similar description is possible in which the state variable describes the oxygen content within a compositionally uniform conduction channel, although the functional dependence on the state variable is likely to be nonlinear. In addition, we neglect any temperature dependence in this static equation in which a Joule heating term would be expected to affect the conductance, most strongly in the insulating portion [30]. Fig. 2(b) shows the resulting fitting of our static model to a range of device low-bias conductance states from 62 μS (16 kΩ) to 2.85 mS (350 Ω), using $a = 3.5 \times 10^{-6}$ S, $b = 3.1$ V^{-1}, and $G_m = 0.02$ S. Data is shown for negative voltages, but the conductance is nearly symmetric in bias.

E. Dynamical Data and Model

The next step in determining the memristor model is to measure the dynamical behavior of the state variable defined above as a function of state and voltage: $dy/dt = F(y, v)$. To do so, we perform time-dependent resistance measurements of Pt/TaO$_x$/Ta memristors in response to voltage steps of varying amplitude and polarity, which produced switching times from 10^{-9} to 10^{0} s. The junction area for the memristors varies from 1×1 μm to 10×10 μm. Separate devices were used for the high bandwidth (<1 μs) measurements of the state and were fabricated on tapered coplanar waveguides as described in [9], and had lower wire resistances to reduce reflections from the 50-Ω source load of the high-speed waveform generator (Tektronix 12-GSa/s AWG). For the high-speed measurements, a real-time Lecroy 820Zi-A oscilloscope is used, while for time scales slower than 1 μs an Agilent B1500 semiconductor parameter analyzer (SPA) is used for both exciting and probing the dynamics.

The effective circuit for both is shown in the inset of Fig. 3, in which $R_{\text{source}} = R_{\text{scope}} = 50\ \Omega$ in the higher speed setup, while being negligible in the SPA setup. In both cases, there is no external current compliance, and the total external resistance (device electrodes, source impedance of generator, and input impedance of measurement unit) plays a large role in controlling the accessible device states.

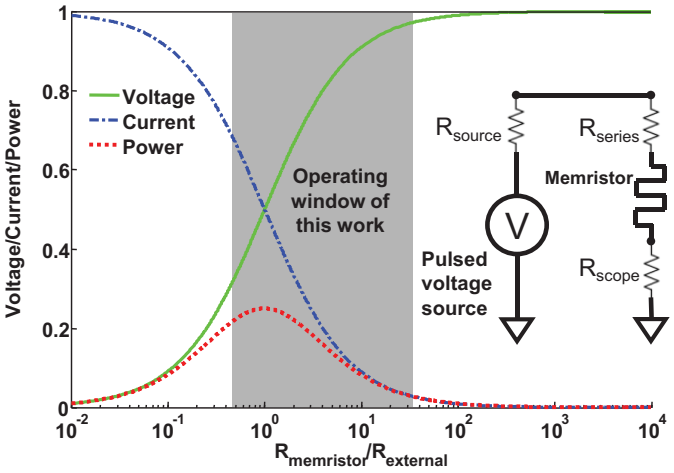

Fig. 3. Normalized plot of memristor voltage, current, and power as a function of the memristor resistance normalized by the total external resistance $R_{\text{ext}} = R_{\text{source}} + R_{\text{series}} + R_{\text{scope}}$. Inset: schematic view of electrical circuit used in dynamics tests. Values for R_{source}, R_{series}, and R_{scope} varies depending on the time scales probed and corresponding memristor electrode width and thicknesses. Time scales <1 μs are probed with a highspeed setup [8], [9] in which $R_{\text{source}} = R_{\text{scope}} = 50\ \Omega$, while longer time scales use a pulsed parameter analyzer in which R_{source} and R_{scope} are negligible.

It is often assumed the series resistance of the circuit containing a memristor is negligible with respect to the ON state of the device. That may, however, not be the case when making probe station measurements on small devices. The voltage divider effect when the memristor and series resistance are comparable can have a major impact on the results of dynamical measurements, and must be carefully factored into the analysis of the data. This is shown in Fig. 3, in which the normalized memristor voltage and current, along with their product, the power, are plotted as a function of memristor state during the application of a constant external voltage. In this plot, only $R_{\text{memristor}}$ is varying. If $R_{\text{memristor}}$ is close in magnitude to the series circuit resistances, the power across the device is largest. As state dynamics dy/dt will likely be a strong function of voltage and internal Joule heating, this shows that a high series resistance can have a significant impact on the measured switching speed. For the following measurements, R_{series} varies between 70 and 600 Ω, dictated by the electrode (wire) thickness, width, and length. The device ON resistance is generally within a factor of two of the external circuit resistance, whereas the OFF resistance is within a factor of ten, and thus the internal device voltage is highly dynamic in itself, and has to be explicitly considered when interpreting the data and constructing a model of the isolated device.

The dynamical evolution during OFF-switching (negative voltage) is shown in Fig. 4(a) and (b) for timescales faster and slower than 1 μs, respectively. The voltage pulse is applied at time $t = 0$ for all data plotted. For each voltage and initial condition, only one representative trace is shown for clarity. The initial ON state is prepared through slow voltage ramps and leads to states that vary from 1.7 mS (580 Ω) to 5.5 mS (180 Ω), and therefore correspond (Fig. 3) to a low-voltage/high-power configuration. The dynamics are a

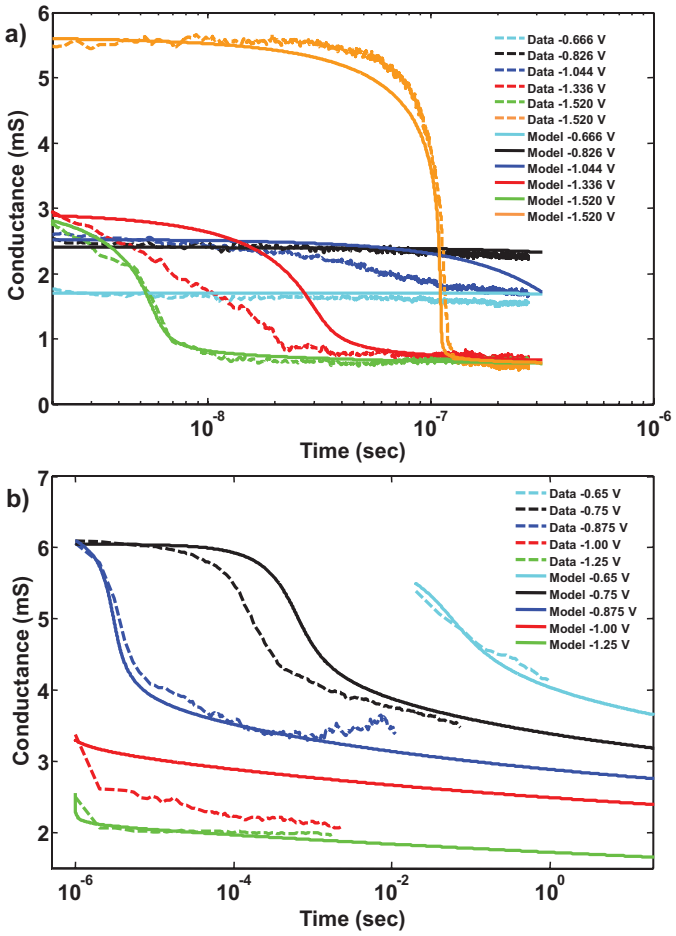

Fig. 4. Measurements (dashed line) and simulations (solid line) of tantalum oxide memristor OFF-switching dynamics with different applied voltages and initial states. Simulation results matching each data curve use the same initial conditions and applied voltage. Model parameters are held constant for all results shown in each panel. (a) Fast OFF-switching using higher speed setup to measure sub-μs dynamics. Memristor probed has a 10×10-μm device area fabricated on a tapered coplanar waveguide. (b) Longer time scale OFF-switching dynamics of a 2×2-μm memristor using a SPA with pulsed voltage generator.

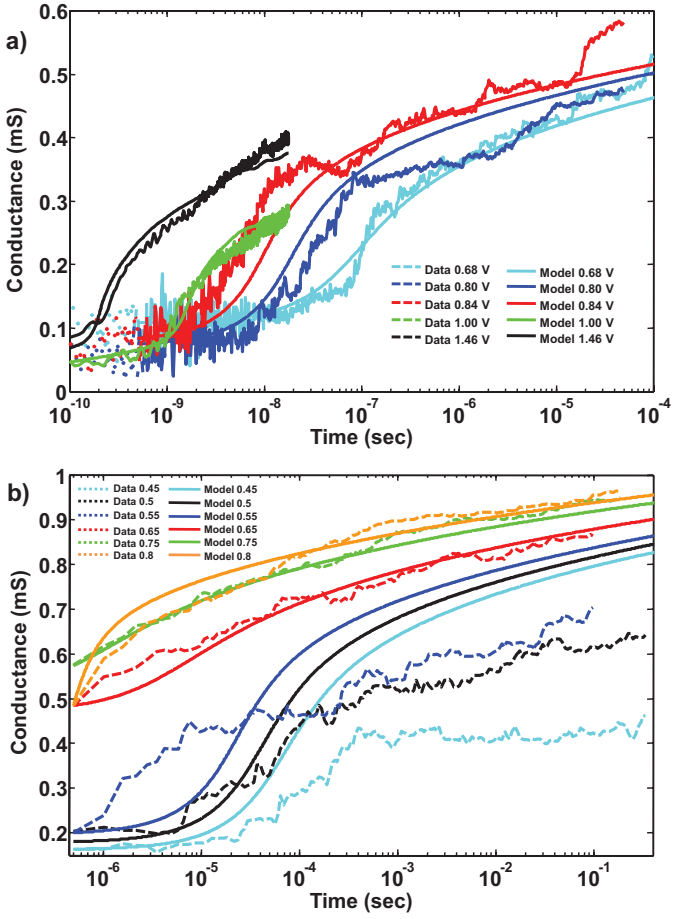

Fig. 5. Measurements (dashed line) and simulations (solid line) of TaO_x memristor ON-switching dynamics with different applied voltages and initial states. Simulation results matching each data curve use the same initial conditions and applied voltage. Model parameters are held constant for all results shown in each panel. (a) Fast ON-switching using higher speed setup to measure sub-μs dynamics. Memristor probed has a 1×1-μm device area fabricated on a tapered coplanar waveguide. (b) Longer time scale ON-switching dynamics of a 1×1-μm memristor using a SPA with pulsed voltage generator.

strong function of memristor voltage: for low applied voltage or high initial conductance (dropping less voltage across the memristor), the initial dynamics is slow. This is shown in Fig. 4(a) with bias amplitude <1.044 V or initial conductance >3 mS. Switching models with a strong voltage dependence are explored, and a good match to the data is obtained with an exponential.

Referring to Fig. 3, as the memristor conductance decreases during OFF-switching, the voltage increases strongly because of the voltage divider effect, and thus voltage-controlled OFF-switching might be expected to continue indefinitely. The data shows that even for applied voltages larger in magnitude than 1.52 V [Fig. 4(a)], the OFF-switching conductance hits a lower limit. Thus, another term is required to include this saturation effect, $\exp[-(y_{\rm OFF}/y)^2]$, where $y_{\rm OFF}$ is proportional to the limiting value of the state variable. This makes physical sense, as a saturation term is needed because of the maximum resistance of the channel when terminally oxidized. Finally, to match the temporal dependence of any individual switching curve, a term dependent on the power, p, is required to slow down the switching, particularly during the initial high power phase of the switching (Fig. 3). The best fit to our data, spanning the full nine decades in time, is found with

$$dy/dt = A \sinh[v/\sigma_{\rm OFF}] \exp[-(y_{\rm OFF}/y)^2] \exp[1/(1+\beta p)] (v < 0). \quad (4)$$

This dynamics model is then computed using the same external voltage, external resistances, and initial memristor state as in the measurement conditions. The resulting simulations are shown in Fig. 4(a) and (b) by the solid lines, showing fairly good agreement with the measured data (dashed lines). The free model parameters, A, $\sigma_{\rm OFF}$, $y_{\rm OFF}$, and β are held constant across each panel for the range of voltages and initial states simulated, with the values provided in Table I.

The dynamical evolution during ON-switching (positive voltage pulses) is shown in Fig. 5(a) and (b) for timescales faster and slower than 1 μs, respectively. As no current compliance is present, a limitation in either highest volt-

TABLE I
MODEL PARAMETERS FOR OFF SWITCHING

			Static Model Parameters			Dynamic Model Parameters			
	Device Size	R_{ext}	a	b	G_M	A	σ_{OFF}	y_{OFF}	β
Fig. 4(a)	10×10 μm	133	3.2 e^{-6}	3	0.02	2.5	0.07	0.091	300
Fig. 4(b)	2×2 μm	70	7.2 e^{-6}	4.7	0.02	8 e^{-11}	0.013	1.163	500

TABLE II
MODEL PARAMETERS FOR ON SWITCHING

			Static Model Parameters			Dynamic Model Parameters			
	Device Size	R_{ext}	a	b	G_M	B	σ_{ON}	y_{ON}	σ_P
Fig. 5(a)	1×1 μm	620	3.5 e^{-6}	3.1	0.02	90	0.10	0.01	2.75 e^{-5}
Fig. 5(b)	1×1 μm	520	3.5 e^{-6}	3.1	0.02	75	0.45	0.02	2.65 e^{-5}

age amplitude or duration of pulse is imposed to avoid high-conductance states that could not be reversed (Stuck ON). In the case of ON switching, the initial high resistance (Fig. 3) implies a high voltage/low power for the memristor. Strong voltage dependence is again observed in the dynamics, but a pronounced onset behavior is also observed—an initial period of slow conductance change followed by rapid switching that does not proceed indefinitely, but saturates. This is evident across the data, particularly for applied voltages 0.68–0.84 V in Fig. 5(a) and 0.45–0.55 V in Fig. 5(b). The rapid switching phase corresponds to a state in which the power dissipated in the memristor rapidly increases, despite the decreasing memristor voltage because of the voltage divider and increasing memristor conductance. Thus, to describe ON-switching accurately, we found that a term with exponential dependence on power is required. The resulting model for ON switching is as follows:

$$dy/dt = B \sin h[v/\sigma_{ON}] \exp[-(y/y_{ON})^2] \exp[p/\sigma_p](v > 0). \quad (5)$$

The results of simulations using the same external voltage profile, external resistances, and initial memristor state as in the measurement conditions are shown in Fig. 5(a) and (b) by the solid lines. Very good agreement is found to the data for the highest voltages, whereas the lowest voltages of Fig. 5(b) begin to diverge, suggesting the model inadequately describes the near-threshold regime $\sim$0.5 V. The free parameters used are provided in Table II. ON-switching has a similar form to the OFF-switching in the voltage dependence, but has an opposite dependence on power in which the Joule heating slows down OFF-switching but speeds up ON-switching. This is not consistent with a thermally assisted process based on absolute temperature, but could be caused by a thermal gradient around the conductive channel that induces radial motion of ions by thermophoresis, which is invoked as a mechanism for unipolar switching [25].

III. MODEL COMPARISON AND RESULTS

In this section, we explore some of the notable features and consequences of our model. A comparison with other models is made and the performance of tantalum oxide-based memristors is evaluated in terms of switching speed, energy cost, and the effects of the circuit environment (wire resistances). Our model has shown a good fit to the dynamics data across nine decades in time and a broad voltage range. Nonetheless, a reasonable extrapolation just outside of this range of data is fruitful to explore some of the expected limits and behaviors.

A. Comparison to Other Metal Oxide Memristor Models

Much like the work presented here, a memristor formalism is used to describe oxide-based resistance switching devices in systems including TiO_2, WO_x, HfO_2, and TaO_x. Metal oxides can support a broad range of transport physics [29], which leads to different models (1) that best describe the system in question. We can roughly divide these into models using resistance switching elements in series ([14], [22], [24]) or parallel ([19] and the present paper). An example of the former is TiO_2, where electrical and physical analysis supports a model with a variable Simmons tunnel barrier, the width of which serves as the state variable [18]. In contrast, similar analysis here leads us to a parallel conduction model for TaO_x with the fractional volume (or cross-sectional area) of the Ohmic element serving as the state variable. In all of the above cases, a strong nonlinearity much like the forms of (4) and (5) in the bias dependence of the state variable's time derivative—e.g., an exponential or super exponential dependence—is observed. This nonlinear dynamics has a number of beneficial technological consequences that are analyzed below for the case of tantalum oxide.

B. Current–Voltage Sweeps

Researchers often plot current–voltage characteristics to quickly display the behavior of a resistance switching device. This can obscure the dynamical nature unless a set of curves at well-specified cycling characteristics are shown. Fig. 6 shows simulation results using our model in response to an applied sawtooth voltage cycle with different sweep rates. The total cycle time varies from 1 s to 10 ns, with a common initial OFF state in all cases, and a voltage sequence of 0, 0.8, 0, -1.2, and 0 V. The simulation results show the characteristic pinched hysteresis loops of a memristor [2]–[4], [18], with the highest frequency cycle yielding a collapsed trace. In all other traces,

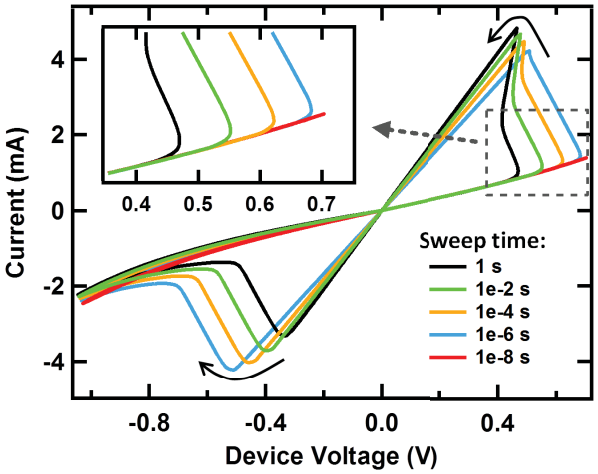

Fig. 6. Simulated results for current–voltage sweeps with varying voltage ramp rates giving a total sweep time from 10 ns to 1 s. A positive voltage sawtooth to +0.8 V is applied followed by a negative sawtooth to −1.2 V. $R_{\text{external}} = 70\ \Omega$, and voltage plotted is the internal device voltage.

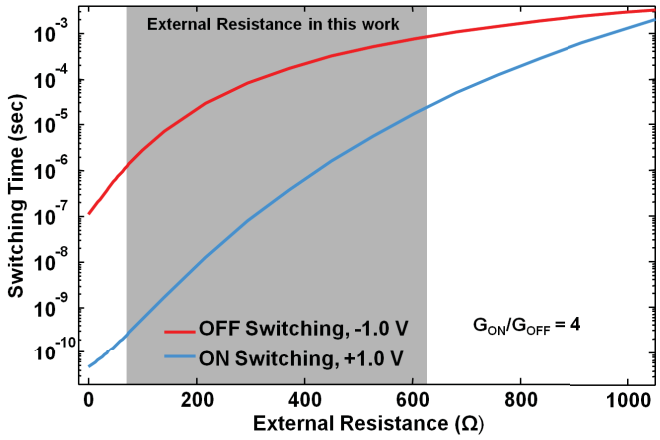

Fig. 7. Simulation result for the switching time dependence on external resistance, using a fixed voltage applied of ± 1.0 V for ON/OFF switching.

the nonlinearity of the dynamics is evident by a steep rise (fall) in the current as the voltage reaches a sufficiently large positive (negative) voltage for ON (OFF) switching to occur within the timescale of the sweep. This dynamical nonlinearity gives rise to an apparent threshold switching voltage, but the value is highly sweep-rate dependent (Fig. 6, inset) as discussed in [31]. The apparent threshold voltage increases with increasing cycle frequency, because the device has less time to switch and does so at higher voltages during the faster cycles. The model reproduces well the current–voltage traces in the actual device, as shown in Fig. 1.

C. Switching Time and Energy

Both ON and OFF switching show an exponential dependence on voltage from (4) and (5). Thus, a very small increase in applied voltage can lead to orders of magnitude faster switching, as observed by other researchers [7], including in the case of tantalum oxide [9]. If the circuit series resistance is close to the ON-state resistance, this will reduce the device voltage and strongly increase switching time.

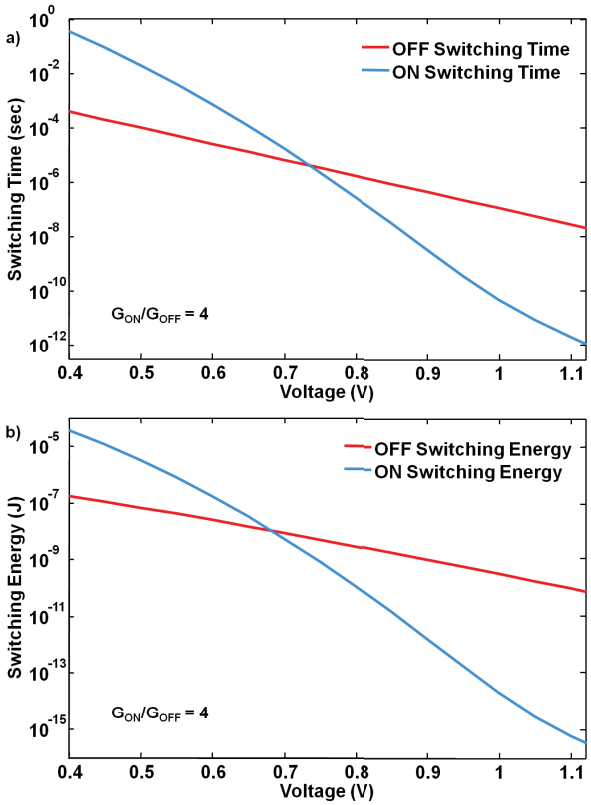

Fig. 8. Simulation results for (a) dependence of switching time on voltage applied for the case of a negligible series resistance and (b) corresponding switching energy. All simulations use a conductance ratio $G_{\text{ON}}/G_{\text{OFF}} = 4$, chosen to match the general operating range in the data from which the model is derived.

To study this issue, we simulate memristor switching over a range of external resistances while applying an external voltage of +1.0 V (to turn ON) and −1.0 V (to turn OFF), and determine the time required to achieve a fixed ON/OFF conductance ratio of four, chosen to closely match the observed operating window of the experimental devices. Fig. 7 shows that the switching time can vary more than seven decades depending on the magnitude of the series resistance. As noted in [32], this is due to the voltage drop across the series resistance. Thus, it is clear that for both characterization and circuit applications, the series resistance should be kept to a minimum to obtain the minimum possible switching time.

Although the devices measured here had a nonnegligible series resistance (70–650 Ω) in the test setup, the derived model allows us to simulate the performance of the devices in circuits where the series resistance is small. In Fig. 8(a), we determine the switching time for a nominal 1-Ω series resistance, and ON/OFF conductance ratio of four. A decrease in switching time with increased voltage is observed for both ON and OFF switching. The different power dependence (going as v^2) in (4) and (5), however, leads to a deviation from strictly exponential behavior for these switching time curves, with the ON switching time having an accelerated voltage dependence. This leads to a crossover of the two curves that is not predicted in the TiO_2 system [14], for which ON switching is always much faster than OFF switching, and is thus not anticipated. This crossover is not studied experimentally.

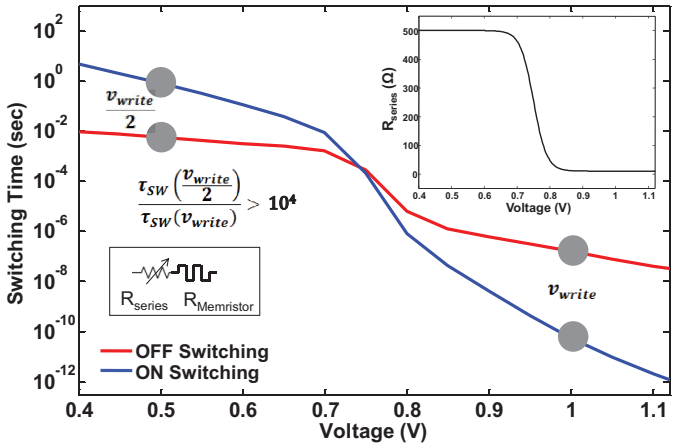

Fig. 9. Simulated switching time versus applied voltage for a TaO_x memristor with a nonlinear series resistor (inset, left) having a resistance varying between 500 and 10 Ω (inset, top right) for voltages less than or greater than 0.75 V, respectively. Using a hypothetical write voltage of v_{write} = 1.0 V, the half selected switching time is over four decades slower for OFF switching and ten decades slower for ON switching

At 1 V, ON switching is predicted to proceed faster than 50 ps, and OFF switching faster than 100 ns. With higher voltage amplitudes, measurements on physical tantalum oxide devices demonstrate 100-ps OFF switching times [9].

We also compute the total energy cost of the ON and OFF switching in the memristor, and the resulting curves in Fig. 8(b) are visually similar to the switching-time curves. Thus, the faster the device switches, the smaller the energy expended. OFF switching at $\leq$10 pJ is possible at reasonable voltage magnitudes, whereas ON switching can get into the hundreds of aJ range. Importantly, the model and parameters developed here are for relatively large micron-scale memristors with currents of a few mA [26] during switching. For smaller devices, the switching voltages remain about the same while the current decreases. Thus, we project that the energy cost for nanoscale devices (with a high device resistance to wire resistance ratio) may be decades lower, and the dominant energy cost is likely to be from capacitive charging/discharging of wires and ohmic losses.

The observations here of a strong voltage nonlinearity [Fig. 8(a), plotted on a log-lin scale] and a strong wire resistance dependence (Fig. 7) can be exploited for mitigating write disturb issues in crossbar arrays. When writing a selected bit, it is desirable to avoid disturbing other bits, particularly those sharing the same row or column and therefore seeing half the write voltage (half-selected bits). Fig. 9 shows that the intrinsic voltage dependence of the dynamics, combined with a nonlinear series resistance that may be fabricated with the devices [13], can strongly mitigate the write disturb issues. If we assume a write voltage of $\pm$1.0 V, the time for a half-selected bit to switch is over four decades longer during OFF switching and ten decades longer during ON switching, therefore providing a comfortable margin.

IV. Conclusion

Analytical approximations to the Chua memristor equations for tantalum oxide resistive switches were determined using static and dynamic electrical measurements and consistency with recent physical characterizations. Both ON and OFF switching showed a predominantly voltage-controlled behavior of exponential form, and an additional power dependence that played an opposite role in the two cases for driving the switching dynamics. ON switching was strongly enhanced by power (local Joule heating), whereas OFF switching was inhibited, consistent with a competing unipolar switching mechanism that may be driven by thermophoresis [25].

We computed the switching times and energy cost for ON and OFF switching as a function of voltage applied to a micron-scale memristor with a negligible series resistance, predicting ps and aJ switching for ON transitions, and ns/pJ for OFF.

With the demonstrated performance of tantalum oxide resistive random-access memory, the compact model developed here is an important step toward simulating large scale arrays of memristors for high-density memory. This predictive model can be used to quantify the bit disturb and interaction issues in such an array, and in developing the appropriate reading and writing circuitry to optimize and evaluate performance. In addition, the physical insight derived from the functional form of the model found here was an important step toward understanding the physical mechanism and further engineering of the devices. Finally, given the similarities in both the material phase diagram and switching behavior for HfO_x and TaO_x, it is likely that these two materials have similar switching mechanisms and the device model developed here may be adapted to HfO_x resistance switching devices.

Acknowledgment

The authors would like to thank W. Jackson and F. Perner for helpful discussions.

References

[1] L. O. Chua, "Memristor-the missing circuit element," *IEEE Trans. Circuit Theory*, vol. 18, no. 5, pp. 507–519, Sep. 1971.

[2] L. O. Chua and S. M. Kang, "Memristive devices and systems," *Proc. IEEE*, vol. 64, no. 2, pp. 209–223, Feb. 1976.

[3] L. O. Chua, "The fourth element," *Proc. IEEE*, vol. 100, no. 6, pp. 1920–1927, Jun. 2012.

[4] L. Chua, "Resistance switching memories are memristors," *Appl. Phys. A*, vol. 102, no. 4, pp. 765–783, Mar. 2011.

[5] J. J. Yang, M. X. Zhang, J. P. Strachan, F. Miao, M. D. Pickett, R. D. Kelley, G. Medeiros-Ribeiro, and R. S. Williams, "High switching endurance in TaO_x memristive devices," *Appl. Phys. Lett.*, vol. 97, no. 23, pp. 232102-1–232102-3, Dec. 2010.

[6] M. J. Lee, C. B. Lee, D. Lee, S. R. Lee, M. Chang, J. H. Hur, Y. -B. Kim, C.-J. Kim, D. H. Seo, S. Seo, U.-I. Chung, I.-K. Yoo, and K. Kim, "A fast, high-endurance and scalable non-volatile memory device made from asymmetric Ta_2O_{5-x}/TaO_{2-x} bilayer structures," *Nat. Mater.*, vol. 10, no. 8, pp. 625–630, Jul. 2011.

[7] H. Y. Lee, P. S. Chen, T. Y. Wu, Y. S. Chen, C. C. Wang, P. J. Tzeng, C. H. Lin, F. Chen, C. H. Lien, and M.-J. Tsai, "Evidence and solution of over-RESET problem for HfOX based resistive memory with sub-ns switching speed and high endurance," in *Proc. IEEE IEDM*, Dec. 2010, pp. 1–4.

[8] Z. Wei, Y. Kanzawa, K. Arita, Y. Katoh, K. Kawai, S. Muraoka, S. Mitani, S. Fujii, K. Katayama, M. Iijima, T. Mikawa, T. Ninomiya, R. Miyanaga, Y. Kawashima, K. Tsuji, A. Himeno, T. Okada, R. Azuma, K. Shimakawa, H. Sugaya, T. Takagi, R. Yasuhara, K. Horiba, H. Kumigashira, and M. Oshima, "Highly reliable TaOx ReRAM and direct evidence of redox reaction mechanism," in *Proc. IEEE IEDM*, Dec. 2008, pp. 293–296.

[9] A. C. Torrezan, J. P. Strachan, G. Medeiros-Ribeiro, and R. S. Williams, "Sub-nanosecond switching of a tantalum oxide memristor," *Nanotechnology*, vol. 22, no. 48, p. 485203, Dec. 2011.

[10] J. P. Strachan, A. C. Torrezan, G. Medeiros-Ribeiro, and R. S. Williams, "The switching location of a bipolar memristor: Chemical, thermal and structural mapping," *Nanotechnology*, vol. 22, no. 25, p. 505402, Jun. 2011.

[11] Z. Wei, T. Takagi, Y. Kanzawa, Y. Katoh, T. Ninomiya, K. Kawai, S. Muraoka, S. Mitani, K. Katayama, S. Fujii, R. Miyanaga, Y. Kawashima, T. Mikawa, K. Shimakawa, and K. Aono, "Demonstration of high-density ReRAM ensuring 10-year retention at 85 °C based on a newly developed reliability model," in *Proc. IEEE IEDM*, Dec. 2011, pp. 1–2.

[12] Y. Yang, P. Sheridan, and W. Lu, "Complementary resistive switching in tantalum oxide-based resistive memory devices," *Appl. Phys. Lett.*, vol. 100, no. 20, pp. 203112-1–203112-4, May 2012.

[13] H. D. Lee, S. G. Kim, K. Cho, H. Hwang, H. Choi, J. Lee, S. H. Lee, H. J. Lee, J. Suh, S. Chung, Y. S. Kim, K. S. Kim, W. S. Nam, J. T. Cheong, J. T. Kim, S. Chae, E. Hwang, S. N. Park, Y. S. Sohn, C. G. Lee, H. S. Shin, K. J. Lee, K. Hong, H. G. Jeong, K. M. Rho, Y. K. Kim, S. Chung, J. Nickel, J. J. Yang, H. S. Cho, F. Perner, R. S. Williams, J. H. Lee, S. K. Park, and S. Hong, "Integration of 4F2 selector-less crossbar array 2Mb ReRAM based on transition metal oxides for high density memory applications," in *Proc. Symp. VLSI Technol.*, Jun. 2012, pp. 151–152.

[14] D. B. Strukov, G. S. Snider, D. R. Stewart, and R. S. Williams, "The missing memristor found," *Nature*, vol. 453, pp. 80–83, May 2008.

[15] J. H. Hur, M.-J. Lee, C. B. Lee, Y.-B. Kim, and C.-J. Kim, "Modeling for bipolar resistive memory switching in transition-metal oxides," *Phys. Rev. B*, vol. 82, no. 15, pp. 155321-1–155321-5, Oct. 2010.

[16] X. Guan, S. Yu, and H.-S. P. Wong, "A SPICE compact model of metal oxide resistive switching memory with variations," *IEEE Electron Device Lett.*, vol. 33, no. 10, pp. 1405–1407, Oct. 2012.

[17] D. Ielmini, F. Nardi, and S. Balatti, "Evidence for voltage-driven set/reset processes in bipolar switching RRAM full text," *IEEE Trans. Electron Device*, vol. 59, no. 8, pp. 2049–2056, Aug. 2012.

[18] M. D. Pickett, D. B. Strukov, J. L. Borghetti, J. J. Yang, G. S. Snider, D. R. Stewart, and R. S. Williams, "Switching dynamics in titanium dioxide memristive devices," *J. Appl. Phys.*, vol. 106, no. 7, pp. 074508-1–074508-6, Oct. 2009.

[19] T. Chang, S. H. Jo, K.-H. Kim, P. Sheridan, S. Gaba, and W. Lu, "Synaptic behaviors and modeling of a metal oxide memristive device," *Appl. Phys. A*, vol. 102, no. 4, pp. 851–855, Mar. 2011.

[20] P. Sheridan, K.-H. Kim, S. Gaba, T. Chang, L. Chen, and W. Lu, "Device and SPICE modeling of RRAM devices," *Nanoscale*, vol. 3, no. 9, pp. 3833–3840, 2011.

[21] S. Menzel, M. Waters, A. Marchewka, U. Bottger, R. Dittman, and R. Waser, "Origin of the ultra-nonlinear switching kinetics in oxide-based resistive switches," *Adv. Funct. Mater.*, vol. 21, no. 23, pp. 4487–4492, Dec. 2011.

[22] J. H. Hur, K. M. Kim, M. Chang, S. R. Lee, D. Lee, C. B. Lee, M.-J. Lee, Y.-B. Kim, C.-J. Kim, and U. Chung, "Modeling for multilevel switching in oxide-based bipolar resistive memory," *Nanotechnology*, vol. 23, no. 22, p. 225702, Jun. 2012.

[23] D. Ielmini, "Modeling the universal set/reset characteristics of bipolar RRAM by field and temperature-driven filament growth," *IEEE Trans. Electron Devices*, vol. 58, no. 12, pp. 4309–4317, Dec. 2011.

[24] D. B. Strukov, J. L. Borghetti, and R. S. Williams, "Coupled ionic and electronic transport model of thin-film semiconductor memristive behavior," *Small*, vol. 5, no. 9, pp. 1058–1063, 2009.

[25] D. B. Strukov, F. Alibart, and R. S. Williams, "Thermophoresis/diffusion as a mechanism for unipolar resistive switching in metal–oxide–metal memristors," *Appl. Phys. A*, vol. 107, no. 3, pp. 509–518, 2012.

[26] F. Miao, J. P. Strachan, J. J. Yang, M.-X. Zhang, I. Goldfarb, A. C. Torrezan, P. Eschbach, R. D. Kelley, G. Medeiros-Ribeiro, and R. S. Williams, "Anatomy of a nanoscale conduction channel reveals the mechanism of a high-performance memristor," *Adv. Mater.*, vol. 23, no. 12, pp. 5633–5640, Dec. 2011.

[27] J. P. Strachan, G. Medeiros-Ribeiro, J. J. Yang, M. X. Zhang, F. Miao, I. Goldfarb, M. Holt, V. Rose, and R. S. Williams, "Spectromicroscopy of tantalum oxide memristors," *Appl. Phys. Lett.*, vol. 98, no. 24, pp. 242114-1–242114-3, Jun. 2011.

[28] F. Miao, W. Yi, I. Goldfarb, J. J. Yang, M.-X. Zhang, M. D. Pickett, J. P. Strachan, G. Medeiros-Ribeiro, and R. S. Williams, "Continuous electrical tuning of the chemical composition of TaO_x-based memristors," *ACS Nano*, vol. 6, no. 3, pp. 2312–2318, Feb. 2012.

[29] I. Goldfarb, F. Miao, J. J. Yang, W. Yi, J. P. Strachan, M.-X. Zhang, M. D. Pickett, G. Medeiros-Ribeiro, and R. S. Williams, "Electronic structure and transport measurements of amorphous transition-metal oxides: Observation of Fermi glass behavior," *Appl. Phys. A*, vol. 107, no. 1, pp. 1–11, Apr. 2012.

[30] A. S. Alexandrov, A. M. Bratkovsky, B. Bridle, S. E. Savelev, D. B. Strukov, R. S. Williams, "Current-controlled negative differential resistance due to Joule heating in TiO_2," *Appl. Phys. Lett.*, vol. 99, no. 20, pp. 202104-1–202104-3, Nov. 2011.

[31] A. Fantini, D. J. Wouters, R. Degraeve, L. Goux, L. Pantisano, G. Kar, Y.-Y. Chen, B. Govoreanu, J. A. Kittl, L. Altimime, and M. Jurczak, "Intrinsic switching behavior in HfO_2 RRAM by fast electrical measurements on novel 2R test structures," in *Proc. 4th IEEE Int. Memory Workshop*, May 2012, pp. 1–4.

[32] D. Ielmini, F. Nardi, and C. Cagli, "Universal reset characteristics of unipolar and bipolar metal-oxide RRAM," *IEEE Trans. Electron Devices*, vol. 58, no. 10, pp. 3252–3253, Oct. 2011.

John Paul Strachan (M'12) received the Ph.D. degree in applied physics from Stanford University, Stanford, CA, USA, in 2007.

He is a Researcher with HP Labs, Palo Alto, CA, USA, and his interests include probing ionic, electronic, and magnetic properties for device applications.

Antonio C. Torrezan (S'04–M'10) received the Ph.D. degree in electrical engineering and computer science from the Massachusetts Institute of Technology, Cambridge, MA, USA, in 2010.

His current research interests include high-speed circuits, memristors, microwave, and THz technologies including vacuum electron devices.

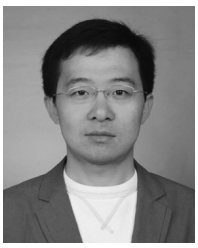

Feng Miao received the Ph.D. degree in physics from the University of California, Riverside, CA, USA, in 2009.

His research group focused on electronic transport properties of novel nanoscale systems, such as memristor and graphene.

Matthew D. Pickett received the Ph.D. degree in materials science and engineering from the University of California, Berkeley, CA, USA, in 2010.

He is a Researcher with Hewlett-Packard Laboratories, Palo Alto, CA, USA.

J. Joshua Yang (M'07) received the Ph.D. degree from the Materials Science Program, University of Wisconsin - Madison, Madison, WI, in 2006.

He is a Principal Researcher with HP Labs, Palo Alto, CA, USA.

Wei Yi received the Ph.D. degree in applied physics from Harvard University, Cambridge, MA, USA, in 2005.

His current research interests include nanoscale materials and device characterization.

Gilberto Medeiros-Ribeiro received the Ph.D. degree in physics from Federal University of Minas Gerais (UFMG) in 1990 and 1996.

Currently, he is a full professor in Physics at UFMG, after positions in Brazilian National Labs and at Hewlett-Packard Labs. He published over 150 papers, awarded 7 US patents and 42 pending.

R. Stanley Williams (SM'08) received the Ph.D. degree in physical chemistry from UC Berkeley, Berkeley, CA, USA, in 1978.

He is an HP Senior Fellow and Vice President at Hewlett-Packard Laboratories. He has >160 US patents and >400 publications in reviewed scientific journals.